Renewable Energy 221 (2024) 119770

Contents lists available at ScienceDirect

Renewable Energy

journal homepage: www.elsevier.com/locate/renene

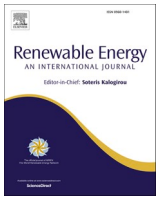

Numerical simulation of the thermal response of seabed sediments to geothermal cycles in Suvilahti, Finland

Marek Mohyla [a], Eva Hrubesova [a], Birgitta Martinkauppi [b], Anne Mäkiranta [b,*], Ville Tuomi [c]

[a] VSB – Technical University of Ostrava, Faculty of Civil Engineering, Department of Geotechnics and Underground Engineering, Ludvika Podeste 1875/17, 708 00, Ostrava, Poruba, Czech Republic
[b] University of Vaasa, School of Technology and Innovations, Energy Technology, P.O. Box 700, 65101, Vaasa, Finland
[c] University of Vaasa, School of Technology and Innovations, Industrial Management, P.O. Box 700, 65101, Vaasa, Finland

ARTICLE INFO

Keywords:
Shallow geothermal energy
Horizontal coaxial pipe
Numerical simulation

ABSTRACT

Renewable thermal energy from seabed sediment is used for heating and cooling houses in Suvilahti, Vaasa, Finland. Innovative coaxial polyethylene pipes (Refla) filled with heat collection fluid are laid horizontally in the sediment layer. This study aims to evaluate the adequacy and possible overuse of this shallow geothermal energy. This entailed a numerical analysis of the heat relations of a "coaxial closed-loop geothermal system (CCGS)" to investigate the thermal behavior of the sediment. The numerical model was developed in Midas GTS NX software with a thermal analysis module. The objective was to understand temperature fluctuation in the sediment, which is influenced not only by geothermal energy exploitation, but also by seasonal weather. The numerical model, due to its design, provided information mainly about changes in sediment temperature due to the geothermal energy exploitation during the different seasons. The results show that in the first third of the total length of the Refla pipes, the sediment environment is significantly affected by energy exploitation's temperature loading. It is advisable to exclude the first third from an analysis of total geothermal energy reserves. The remaining two-thirds of the length shows potential to provide sustainable, long-term geothermal energy (GE) exploitation at the current rate.

1. Introduction

Exesive production of greenhouse gases and the increase in humanity's anthropogenic footprint on Earth is a major societal issue [1–5]. One way to mitigate this footprint is to reduce CO_2 production by using "emission-free" energy sources [6–8]. This renewable energy underpins development of low-carbon energy supply systems [9]. Europe has set ever-tougher targets to increase the share of renewables in energy production [10,11]. Traditional fossil energy sources are also a finite resource [12]. Geothermal energy derived via deep vertical boreholes has been used for several decades [13–15], and Finnish geological conditions make it suitable for heating and cooling buildings [16]. However, shallow geothermal energy can be stored in sediments in seasons with sufficient heat, providing another source of energy.

One method of utilizing shallow geothermal energy is to exploit it from the seabed sediment [17]. The suburb of Suvilahti in Vaasa, Finland, began to collect thermal energy from seabed sediment for 42 houses in 2008 [18]. The pilot system was planned and implemented rather quickly due to the need to meet the tight schedule of the local Vaasa Housing Fair project. Using new Refla pipe (RP), this installation has been a source of enthusiasm for researchers ever since. The term "Refla" is a product name/brand established by a Finnish company which owner invented that coaxial pipe. This innovative "flower" pipe consists of one central pipe and five external chambers. Girgibo et al. [19] concluded that sediment heat energy can be considered as a prominent source of renewable energy, making a useful contribution to reduction of climate change, at least in summer. This paper assesses the potential for using a numerical analysis of the heat relation of a "coaxial closed-loop geothermal system (CCGS)" of the type implemented in Suvilahti. The system's 300 m-long pipes are placed horizontally at a depth of about 3.5 m in seabed sediments, in two fan-like configurations. Unlike traditional geothermal vertical boreholes, this arrangement is significantly affected by seasonal temperature changes due to the modest depth of the pipes in the seabed sediments [20–24]. The novelty of this study is to simulate actual measured temperature data in order to evaluate the adequacy of seabed sediment heat and investigate its possible overuse in the long term.

* Corresponding author.
E-mail address: anne.makiranta@uwasa.fi (A. Mäkiranta).

https://doi.org/10.1016/j.renene.2023.119770
Received 20 November 2022; Received in revised form 23 November 2023; Accepted 28 November 2023
Available online 4 December 2023

Nomenclature

A	amplitude (°C)
A_{out}	cross-sectional area of outer chamber (mm^2)
A_{in}	cross-sectional area of inner chamber (mm^2)
c_p	specific heat (J/kg.K)
E	energy (PJ/year)
f	frequency (Hz)
k	conductivity (W/(m.K))
t	time (day, year)
T	temperature (°C)
T_{base}	temperature at the base of numerical model (°C)
T_{init}	initial temperature of the numerical model (°C)
T_{top}	temperature at the top of the numerical model (°C)
T_1	fluid temperature in the outer chamber along the length of the Refla pipe (°C)
$T_{1(0\ m)}$	inlet fluid temperature in the outer chamber of the Refla pipe (°C)
T_2	fluid temperature in the return branch of the Refla pipe (inner chamber) (°C)
$T_{2(0\ m)}$	outflow fluid temperature of the return branch of the Refla pipe (inner chamber) (°C)
T_3	fluid temperature monitored along the length of the Refla pipe using optical fibers (°C)
$T_{3(0\ m)}$	temperature monitored at the start of the Refla pipe using optical fibers (°C)
Y	shift (°C)
z	vertical direction (m)
φ	phase (day)
$\Delta T_{(A\text{-}A)}$	temperature difference between inner and outer fluid in the Refla pipe at the shore (°C)
$\Delta T_{(B-B)}$	temperature difference between inner and outer fluid along the Refla pipe (°C)
$\Delta T_{(C-C)}$	temperature difference between inner and outer fluid at the end of Refla pipe (°C)
CCGS	coaxial closed-loop geothermal system
CO_2	carbon dioxide
DTS	distributed temperature sensing
FEM	finite element method
GE	geothermal energy
GHE	Ground heat exchanger
PE	polyethylene
RP/RPs	Refla pipe/s

The numerical model was developed in Midas GTS NX software version 2021 with a thermal analysis module. The input data were monitoring results from 2013 to 2016. Temperatures in the near field along the RP were measured using the distributed temperature sensing (DTS) method [25–27]. The liquid temperature at the RP outlets was also monitored. The data were used to develop the model's loading at the prescribed temperature. The numerical analysis evaluates the fluctuation of the temperature field in the sediment. It shows that the temperature field is influenced not only by the exploitation of the geothermal energy, but also by seasonal temperature changes [28–34]. These seasonal changes are so significant, that in order to understand their effects on the sediment field's temperature, they necessitated development of a numerical sub-analysis that excluded geothermal energy exploitation. Subsequently, a final thermal loading model was implemented in which GE exploitation was also activated. The modeled solution employed a set of three two-dimensional (2D) cross-sections at one-third, two-thirds and at the end of the RP. The temperature loading of each 2D model corresponded to the monitored values at the equivalent distance along the pipes. The simplicity of a 2D model allowed it to accurately handle the specific axial cross-section of the RP. The model provided sufficient information about the temperature changes in the near region around the RP. Finally, the sediment environment was loaded with the prescribed temperature in the numerical model. This step makes it possible to evaluate the temperature evolution in the sediments during use and to estimate the installation's long-term thermal stability.

1.1. Ground heat exchanger coaxial pipe as an innovation

A ground heat exchanger (GHE) is a typically pipe placed into the ground allowing heat to be exchanged between the ground and a fluid circulating within the pipe. Alternatively, there are various geometrical forms of coaxial pipes: pipe-in-pipe, multi-pipe, or multi-chamber (Fig. 1) [35]. GHE pipe-in-pipe consists of a central pipe inserted into a larger external pipe, forming an annular flow channel between them, as shown in Fig. 1(a). A multi-pipe design, Fig. 1(b), consists of a central pipe connected at the bottom of with several smaller external and independent flow channels. A multi-chamber GHE is similar to the multi-pipe design, except that the central pipe and the external channels or chambers are integrated into a single pipe structure, as shown in

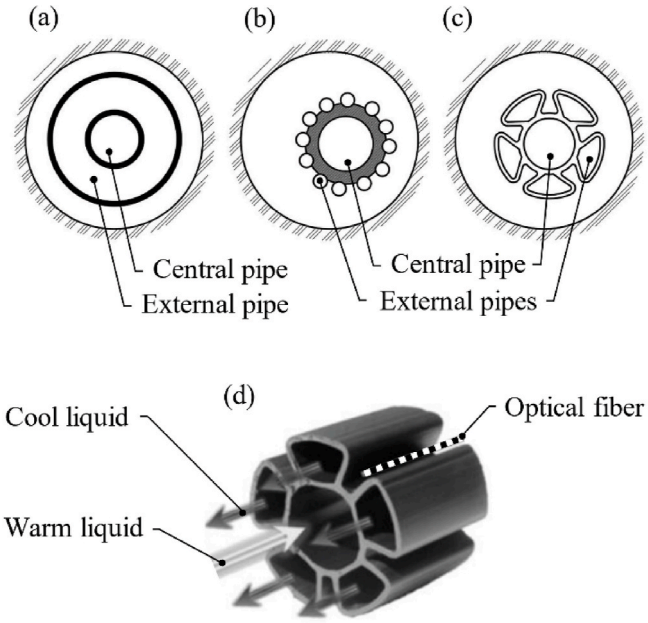

Fig. 1. Illustration of different types of coaxial GHE geometrics [35].

Fig. 1(c and d). The focus of this study, the Suvilahti installation, uses an innovative multi-chamber GHE pipe. This was implemented in only a few sites in Finland and Sweden around year 2007. Unfortunately, this particular Refla pipe (RP) product did not succeed due to disagreements within the company's management, although the technology was working properly.

The diffusion of so-called "green" energy technologies has been widely studied, including solar water-heating [36], small-scale renewable energy [37], renewable heating technologies [38,39] and other sustainable product innovations [40]. The multi-chamber pipe studied in this paper is the kind of innovation which is supposed to be quite acceptable as a supplementary heating system for Finnish houses [41]. An innovation's acceptance depends on its relative advantage, i.e., the

degree to which it is perceived as better than the idea it supersedes. Is it more productive, efficient, profitable or better than existing practices in some other way? The diffusion of the innovation is also affected by current values, past experiences and the needs of the market. Potential adopters should be able to understand and observe the relative advantages of the new technology. Trialability - the degree to which an innovation may be tried on a limited basis - is also a determinant [42].

1.2. Suvilahti area

Vaasa Housing Fair took place in Suvilahti, a suburb of the Finnish coastal city of Vaasa in 2008. A section of this residential area was designed to harness the annually reloaded heat energy from the seabed sediment, using it as heating and cooling energy. The energy is mainly generated by the Sun. The unique low-energy network was designed to cover the heating and cooling demand of 42 detached houses. The heat collection pipework, which totaled almost 8 km, comprised two fan-shaped arrangements of 300 m-long pipes, one with 12 pipes, the other with 14. The two sets of pipes were installed horizontally into the solid clay layer of the seabed sediment in the Gulf of Bothnia (Fig. 2).

They were set 3–4 m below the surface of the seabed. The heat derived from the sediment and collected by the fluid circulating in the pipework is increased with heat pumps inside the houses. The system is also used for cooling houses in the summer. Mäkiranta et al. [43] have researched the correlation between air, sediment and heat carrier liquid temperatures. They observed a high correlation when sediment temperatures were compared to the previous month's heat carrier liquid temperatures. Heat carrier liquid and sediment temperatures of the same month also correlated strongly. Sediment temperatures were indicating the previous weather conditions. The sizing of the installed system was observed to be sufficient. The main network of Suvilahti's low energy system has 12 distribution wells to serve heating and cooling energy to the 42 houses in the project. The heat carrier fluid runs in each of the pipe's outer chambers, gathering thermal energy. When the fluid reaches the end of each pipe, it returns in the central pipe to the shore where it releases its thermal energy for the heat pumps. Then the fluid starts the cycle again. The optical fiber cable for monitoring sediment temperatures was attached to the side of the heat collection pipes, as shown in Fig. 1.

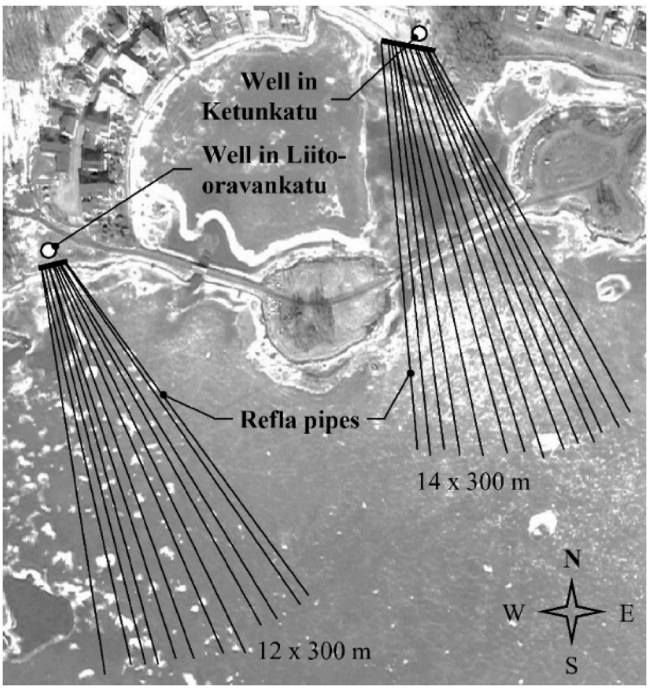

Fig. 2. Suvilahti shallow energy network (citation of idea adopted from Vaasan Vesi).

2. Methods and case study

Fig. 3 provides a flowchart of the current study. It is divided into two sections. The one on the left describes the procedure for assembling and calibrating the numerical model without a thermal load (initial state determination). This step is important in terms of optimizing the boundary conditions and the model's initial temperature. If seasonal monitored data before exploitation of geothermal energy are available, they can be used for model calibration. Unfortunately, this type of monitored data were not available for this study.

The correct setting of the initial temperature (T_{init}) of the model also significantly affects the results of the model: this is discussed in more detail in chapter 2.3. Once the numerical model is calibrated and its behavior accords with the assumptions or is consistent with monitored data, then a thermal load can be applied (right side of the flowchart). Subsequent comparison of the numerical model's results with the monitored data will give a basic idea of the relevance of the applied thermal load. If results are inconsistent, it is possible to redesign the thermal load element and repeat the process.

2.1. Description of the numerical model

The aim of the numerical model is to clarify the behavior of temperature fluctuation in the Suvilahti seabed sediments used as a reservoir of geothermal energy. Geothermal energy is exploited using a specific coaxial RP, placed sub-horizontally parallel to the relief of the seabed at a depth of about 3.5 m. The 300 m-long RPs are in two fan configurations, with a combined total of 26 pipes. The expected widths of the fans at their ends are about 155 m and 165 m. The axial spacing of the RPs are as follows:

- the average axial spacing between the pipes at the shore is 2 m,
- at the distance 300 m from the shore, i.e., at the end of the RP, the average axial spacing is 14 m,
- intermediate spacings are linearly interpolated.

The model was created in Midas GTS NX finite element method (FEM) software with a thermal analysis module. A 2D variant of the model was chosen to capture in detail the real cross-section of the RP. The 2D model assesses the thermal gradient in cross-section to the longitudinal axis of the RP.

The model's height is 7.5 m. This comprises 3.5 m from the RP to the surface of the seabed sediment, plus 4 m below the RP. The width of the model varies in 2 m-steps from 4 m to 14 m, correlating with the fan-shaped RP configurations. The variable width of the model allows cross-sectional simulation of sediment temperatures at different axial measurements along the length of the RPs. Sediment temperatures were modeled at 100 m, 200 m, and 300 m along the RP, measured from the shore.

Fig. 4 depicts the finite element mesh of the model. The blue and green lines represent the boundary conditions, presented in chapter 2.2.

The model's heat transfer analysis simulates almost 10 years of heat flow in the area around one RP. Heat transport is ensured by conduction. The sediments are 100 % saturated. Groundwater flow is not considered in the calculation. The time step of the simulation is 30 days and 120 steps have been computed, representing the passage of 3600 days. The RP consists of five outer chambers carrying the input fluid used for collecting thermal energy from the sediment, plus an inner chamber for fluid return. The outer and inner chambers are thermally affected by each other, which is the reason for choosing a 2D model able to capture the shape of the RP. Table 1 lists the thermal properties of the materials; RP, fluid and seabed sediment [1]. The fluid, a mixture of water and ethanol, has a frost resistance of −15 °C. The sediment layer in Suvilahti

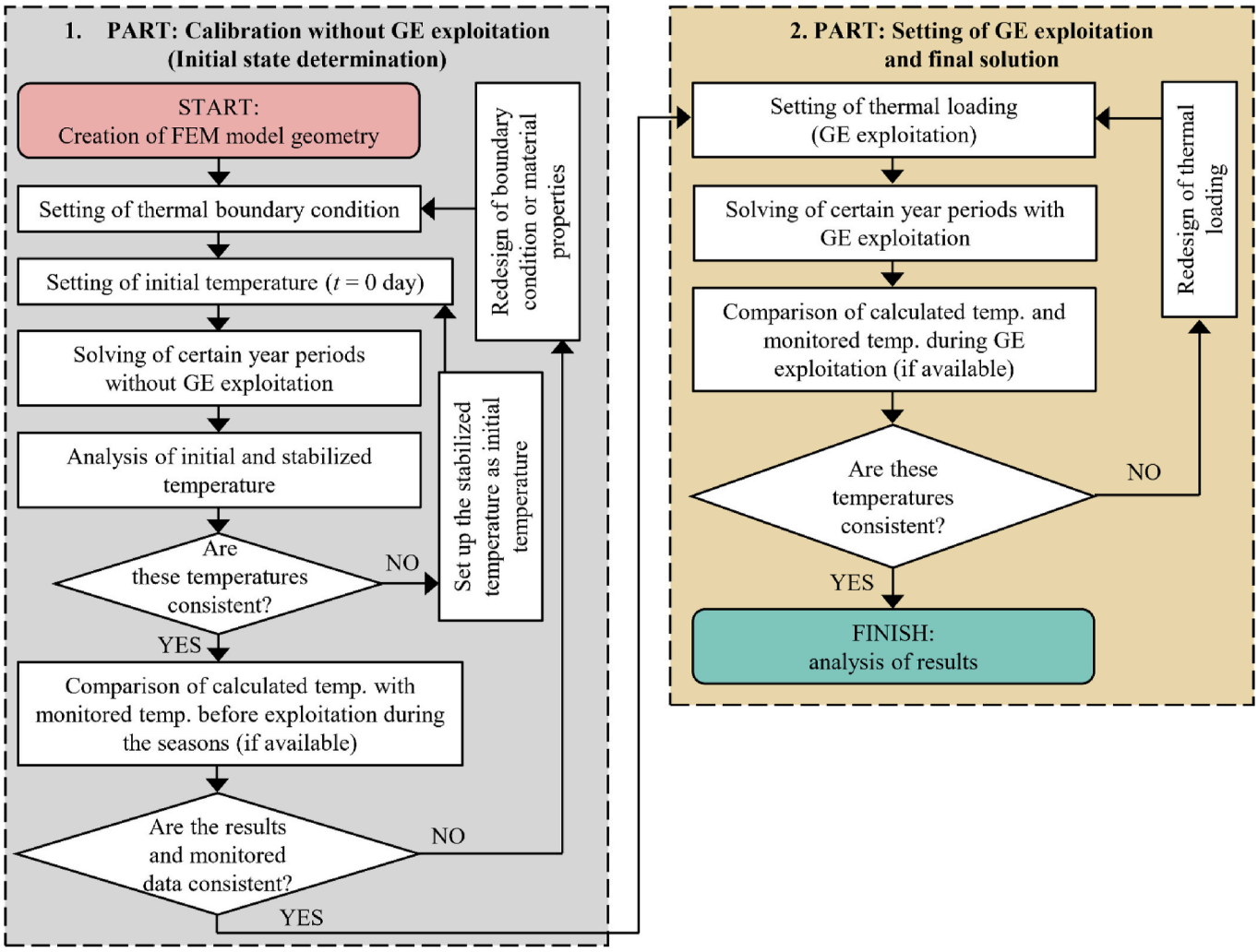

Fig. 3. Flowchart of numerical approach. (color figure).

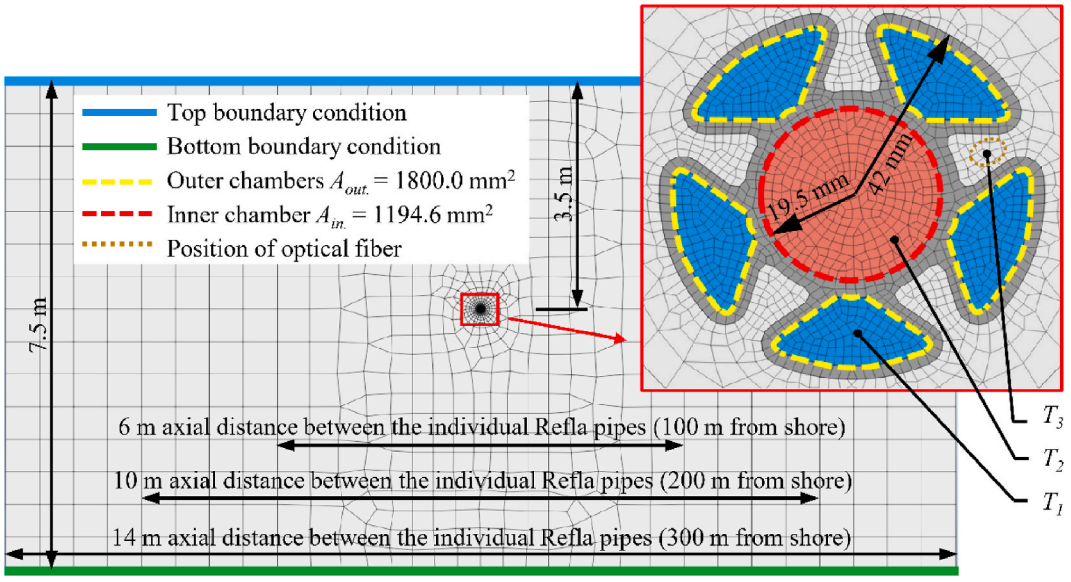

Fig. 4. Finite element mesh, with Refla pipe mesh in detail. (color figure).

Table 1
Thermal properties of materials [23].

Material	Conductivity [W/(m.K)]	Specific Heat [J/kg.K]
Refla pipe (RP)	0.45	2000
Fluid	0.25	3250
sediment	0.86	1400

at a depth of 0–3 m is composed of sulfide muddy clay; it is solid clay at 3 m and beyond [44]. The RP is made of polyethylene [37].

2.2. Determination of thermal boundary conditions

Thermal boundary conditions are an essential element of numerical modeling. They can be understood as describing the thermal behavior of the immediate surroundings outside the modeled area, which has a significant effect on the behavior of the model itself. Consideration of boundary conditions is essential for the numerical model as a whole. In long-time numerical simulations that must take account of seasonal effects, the thermal boundary conditions are particularly important. The following boundary conditions were applied in this model:

- Prescribed temperature $T_{base} = 8$ °C was applied at the base of the model (green line in Fig. 4) [20]. This constant temperature is assumed for all computational steps throughout the 10-year simulation. The temperature $T_{base} = 8$ °C was assumed from Ref. [44], where temperature profile of the sediment in Suvilahti area is published. The temperature profile corresponds to the measurements in 2006. The temperature of 8 °C is specific for depth 7.5–8 m in sediment during whole year.
- Top of the model, i.e., the seabed (blue line in Fig. 4), must accommodate a variable temperature, T_{top}, described by a sine curve. The measured temperature oscillates between 2 and 14 °C [43]. The maximum temperature is observed in August. Presumption: this temperature is variable only with time, not with location of analyzed cross-sections, because the seawater flow ensures a constant temperature across the whole seabed. The sine function of the seabed temperature is as follows formula (1):

$$T_{top} = Y + A \bullet sin\left(2 \bullet \pi \bullet \frac{1}{f} \bullet t + \varphi\right) \quad (1)$$

where:
$Y = 8$ °C shift,
$A = 6$ °C amplitude (temperature oscillation between 2 and 14 °C (8 ± 6 °C),
$f = 360$ Hz frequency (one oscillation per 360 days),
t time,
φ phase.

- The sides of the model are not treated by any boundary condition, i.e., without heat loss or gains.

2.3. Determination of initial temperature of model

Initial temperature T_{init} of the model is the sediment temperature at time $t = 0$ days in simulation. The model's initial temperature is constant, but in a reality it is a function of depth and time, as shown in next chapter (Fig. 7). In the top part of the sediments there are not two places at different depths with identical temperature at the same time. Equally, nowhere in the top part of the sediment has the same temperature during different seasons. For this reason, a first partial parametric study of initial temperature was carried out. This evaluated the development of this temperature in the RP position for a period of ten years. It was always evaluated as a turning point between years of simulation. The expected average installation depth of the RP is 3.5 m.

At this depth, it was assumed that temperature would fluctuate in the range of 6–9 °C and average 7.5 °C. To verify this, a symmetric initial temperature interval of 0–15 °C was used with four values in steps of 5 °C and an average value 7.5 °C. This is shown in Fig. 5. The results of the first partial study show that the correct initial temperature also has a significant effect on the results. It is evident from Fig. 5 that the sediment temperature at the RP depth was stabilized after about five years at 8.2 °C. This value was subsequently used as an ideal initial temperature for numerical simulation.

2.4. Analysis of origin temperature in Suvilahti sediments

Fig. 6 illustrates the change in sediment temperature over one year of simulation. The dotted line (with circle mark) demonstrates the boundary temperature condition $T_{top} = f(t)$ at the top of the model, i.e, the seabed. It is the same for each year of simulation. The dashed line (with diamond mark) demonstrates the temperature oscillation at the depth of the RP. The solid line (with triangle mark) shows the boundary condition at the model's base ($T_{base} = 8$ °C). The temperature at a depth of 1.5 m below the seabed is also shown by dashed line (with square mark). All the curves exhibit a sine function shape, but each has a different property, due to the variation of delay in the seasonal-related warming of the sediments at different depths.

Fig. 7 shows the temperature development in the sediment layer during the last year of simulation, without GE exploitation. The typical fan shape is a consequence of the seasonal surface temperature fluctuation. It can be said that this temperature development is also a significant implicit initial condition of the model, and dependent on those real explicit boundary conditions. Temperature monitoring in sediments indicates that the temperature at a depth of 3–4 m is already consistent [20]. It can be concluded that the boundary conditions, including material characteristics, were used correctly.

Boundary conditions, together with the set initial temperature and model geometry, represent the basic 2D space, which respects the temperature conditions in the studied area, including surface seasonal climatic changes. These temperature conditions are known in space and time. The analysis of the initial temperature and the boundary conditions showed that the numerical model in the case study needs about five years for stabilization of origin thermal regime (see chapter 2.3). In research involving shallow areas, time-related change of climatic conditions have a significant affect and so are a critical factor. This is not a factor for vertical geothermal heat pump systems, where the dominant element is depth and its increasing temperature gradient. Conversely, in the presented model of the shallow area, depth-related increase of the temperature gradient is not a factor and so is not considered.

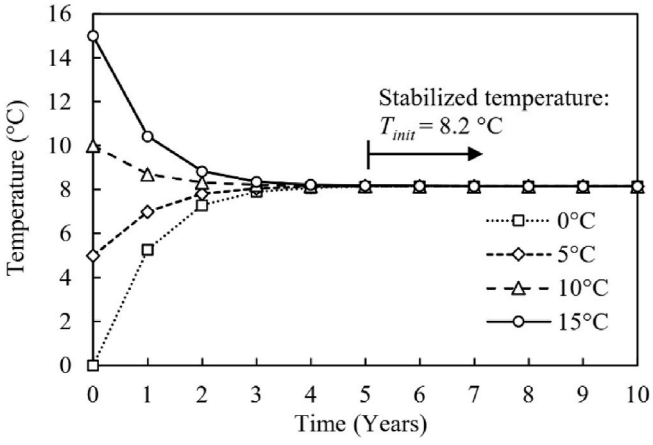

Fig. 5. Temperature development in the place of Refla pipe affected by the initial temperature of the model (10 years of simulation).

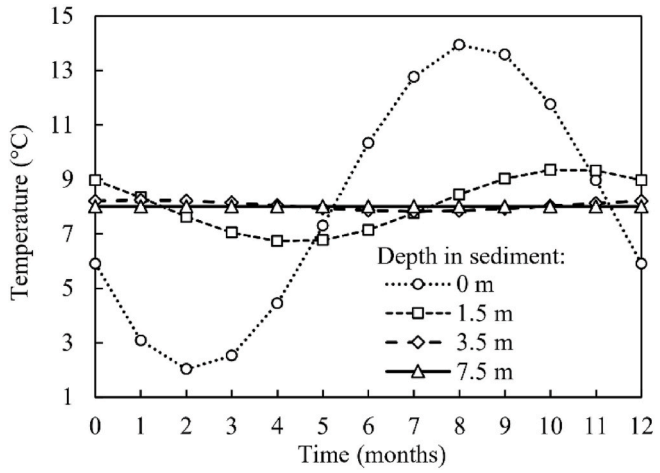

Fig. 6. Dependence of the initial sediment temperature over time in a numerical model.

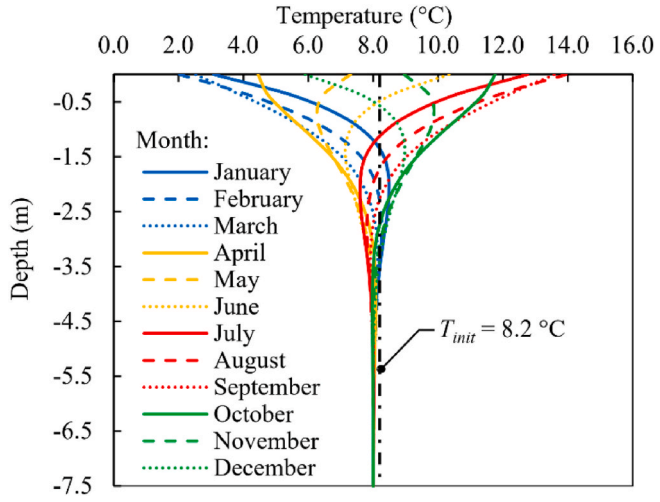

Fig. 7. Demonstration of origin temperature development in sediments during the 10th year of the simulation (without GE exploitation). (color figure).

2.5. Analysis of thermal loading

The model described above was loaded by "prescribed temperatures" based on monitored data from the RP (Fig. 8). The values used were the average fluid temperatures from years 2013–2016, smoothed by a polynomial function with two variables (in "distance from shore" direction). Together with the temperature at the RP outlet, these are the only monitored values.

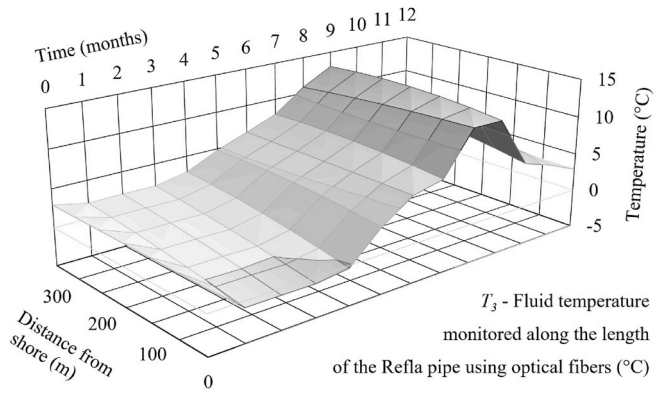

Fig. 8. Temperatures along the Refla pipe (based on monitored data in 2014).

The enlarged portion of Fig. 4 depicts the finite element mesh of the RP. The yellow and red dashed lines represent the boundary of the areas over which the sediment environment is thermally affected, i.e, areas where geothermal energy is exploited. The following labels are used in this study:

T_1 – fluid temperature in the outer chamber along the length of the RP (°C);
T_2 – fluid temperature in the return branch of the RP (°C);
T_3 – fluid temperature monitored along the length of the RP using optical fibers (°C).

Fig. 9 is a schematic depiction of the RP's layout and temperature conditions. Section A-A′ represents the start of the pipe, section C–C′ represents the end of the pipe, and section B–B′ represents any intermediate point along the pipe. The dotted line represents the knowledge of the monitored temperature T_3 in the entire length of the pipe.

There is a relationship between temperatures T_1 to T_3, but it is an equation with three unknowns. At the start of the RP, the temperature $T_{3\,(0\,m)}$ (monitoring) and $T_{2(0\,m)}$ (outlet temperature) are known by actual measurement.

Applying these data, a second partial study was carried out to find the temperature $T_{1(0\,m)}$, and thus define the relationship between temperaturesmT_1 to T_3. The geometric conditions between the individual chambers of the RP were considered, including the material characteristics of the individual materials (see Fig. 4).

In a further partial study, the temperatures $T_{1(0\,m)}$ and $T_{2(0\,m)}$ are known, and temperature $T_{3(0\,m)}$ is determined. Fig. 10 summarizes the results obtained in graphic form.

The procedure is as follows: the initial temperature T_3 is located on the horizontal axis, which is monitored. Furthermore, the known temperature T_2 allows the determination of temperature T_1, which is read on the vertical axis. This can be applied to determine the temperatures T_1 and T_2, based on the knowledge of the temperature T_3 at any distance of the RP.

However, the temperature T_2 is known only at the outlet of the RP, not elsewhere. During the next solution, the following assumptions were made:

- It can be said with certainty that the temperatures T_1 and T_2 are identical at the end of the RP.

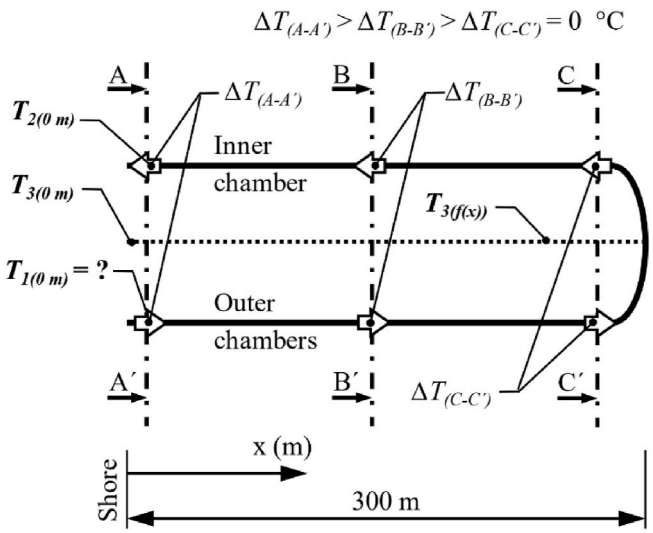

Fig. 9. Conceptional diagram of Refla pipe loop.

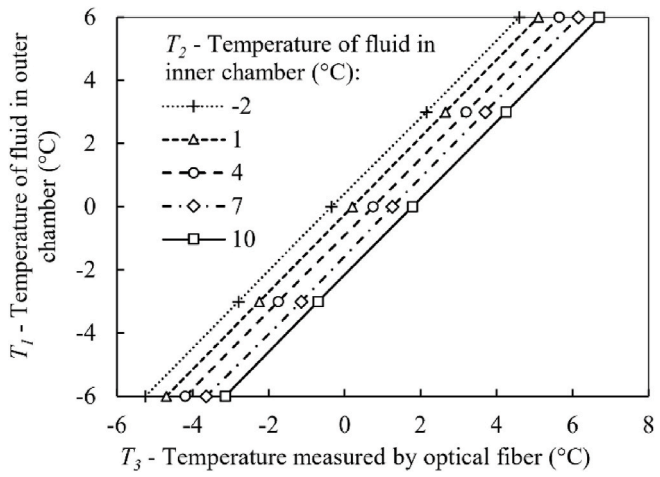

Fig. 10. Temperature dependence T_1, T_2 in Refla pipe cross-section and T_3 outside the Refla pipe.

- It is assumed that at the end of the RP the liquid temperature (T_1 and T_2) is the same as the ambient temperature (T_3), i.e., $T_1 = T_2 = T_3$. This phenomenon is considered in the model at the end of the RP, which is borderline in terms of the sustainability of the geothermal system. In fact, this phenomenon, when the temperature of the input fluid warms up to ambient temperature, may occur before the end of the pipe. With excessive exploitation of geothermal energy, this imaginary point can shift without it being possible to observe this phenomenon.
- temperature T_3 (fiber-optic monitoring) is known throughout the length of the RP. According to the second partial parametric study, temperatures T_1 and T_2 can also be determined along the RP's length.

The main portion of Fig. 11 shows the development of temperatures during the year.

The solid lines represent T_1 and T_2 at 100 m distance from shore; the dashed lines depict T_1 and T_2 at distance 200 m from the shore. The dotted line describes temperature T_1 and T_2 at 300 m from shore, which are the same. Results of an earlier study [19] showed that the best distance for sediment heat energy production in summer is between 100 and 190 m (sediment temperature recording, measured distance from shore). However, this seemed to depend on the month in which the data were collected.

The right-hand part of Fig. 11 depicts the relationship between temperatures T_1 to T_3 along the RP in November. Temperature T_3 (dotted line), is based on fiber-optic monitoring. Temperature T_2 at a distance of 0 m is the temperature at the outlet of the RP and is also the result of monitoring. Based on the assumption $T_1 = T_2 = T_3$ at a distance of 300 m (at the end of the RP), the temperatures along the entire RP can be estimated.

3. Results and discussion

Fig. 12 depicts the model's sediment temperature data in axial distance from shore (at 100 m, 200 m, and 300 m) and in radial axis from the RP. The results from the simulation's final (tenth) year were used. The results should be understood as a comparison of sediment temperatures before and during GE exploitation. This comparison will provide an overview and highlight features or areas that are subjected to higher temperature loads than are appropriate for the sustainability of the geothermal resource.

The a) plot in Fig. 12 shows sediment temperature distribution during the year at 100 m from shore. At this point, adjacent RPs are 6 m apart, so the radial distance on the X-axis extends only to 3 m, the axis of symmetry (shown as a vertical dot/dash black line). The horizontal dashed lines at 7.7 °C and 8.3 °C (average 8.0 °C) define the envelope of temperature fluctuations during the different seasons, without geothermal energy exploitation. This envelope is specific for the RP's depth of 3.5 m (see chapter 2.4). The colored lines represent the sediment temperatures in the geothermal exploitation regime during each month of the last year of the simulation. The year's average is also depicted, shown as a black dot-dash line.

Similarly, the b) plot of Fig. 12 depicts the model's equivalent data at 200 m from shore; the c) plot illustrates the data for the end of the pipes, 300 m from the shore. The vertical dot-dash line on the right of each plot represents the axis of symmetry. At 200 m from shore this is at 5 m because adjacent RPs are 10 m apart; at 300 m from the shore adjacent RPs are 14 m apart, so the axis of symmetry is at 7 m. For analysis of the study's results, the sediment exploitation regime has been divided into three zones, reflecting different degrees of influence on the initial temperature as a consequence of energy exploitation. The basis for the comparison is the year's average sediment temperature at each location:

- high impact: more than 10 % variance with initial average temperature,
- low impact: 2 %–10 % variance with initial average temperature,
- zero impact: less than 2 % variance with initial average temperature.

At 100 m from the shore (Fig. 12, left-hand plot), all radial distances between adjacent RPs meet the above definition of high impact. The sediment temperature reductions as a consequence of energy exploitation is 2.7 °C at the RP and 0.8 °C at the edge of model, 3 m away. At 200 m from the shore (Fig. 12, central plot), adjacent RPs are 10 m apart. The high impact zone reduces to 1.7 m radial distance from the RP, and the temperature drop is 2.3 °C at the RP and only 0.6 °C at the limit of the

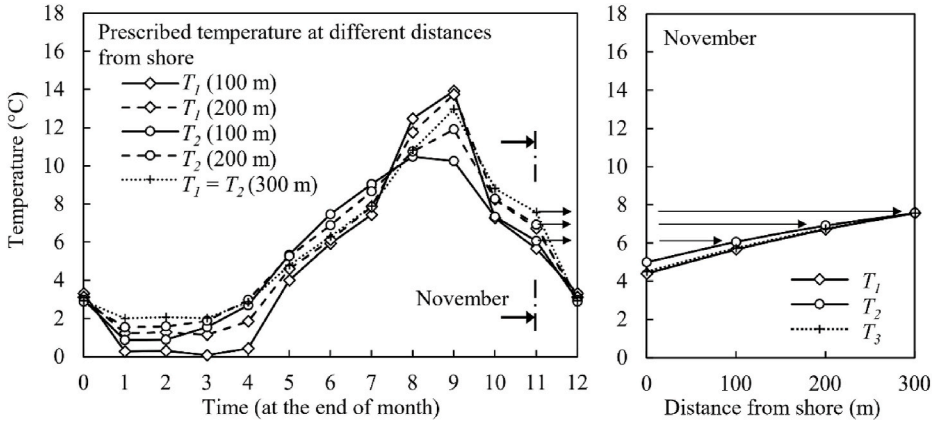

Fig. 11. Time dependence of T_1, T_2 and T_3 temperatures during the year.

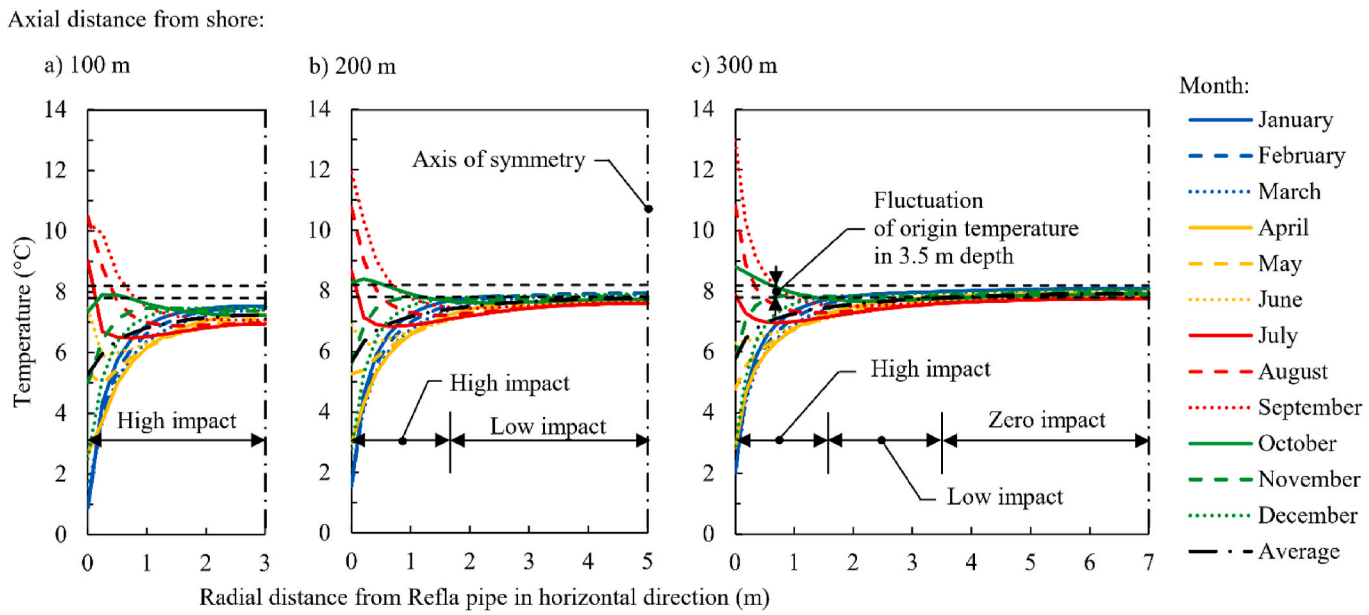

Fig. 12. Temperature distribution in radial distance from Refla pipe in horizontal direction. (color figure).

high impact zone, 1.7 m away. There is a low-impact zone beyond this point, with a temperature drop ranging from 0.5 °C at the nearest edge to 0.2 °C at 5 m radial distance from the RP. At the end of the RP, 300 m from the shore (Fig. 12, right-hand plot), the above trend of reducing impact continues. The high-impact zone has again decreased, but not significantly, to a radial measurement of 1.6 m. The drop in average sediment temperature in this zone is 2.2 °C at the RP and 0.5 °C at the zone's edge. In the low-impact zone, i.e., 1.6 m–3.5 m radial distance, temperature reductions range from 0.4 °C to 0.2 °C respectively. A zone of zero impact exists beyond 3.5 m, where the temperature drop is less than 0.2 °C. Table 2 tabulates these results.

Analysis of the temperature fluctuations in the horizontal axis of the 2D cross-sections shows several facts that should be understood in more qualitative terms. The 2D cross-section at 100 m from the shore showed that the axial spacing of adjacent RPs is small enough to cause appreciable interference, and thus significant decrease in sediment temperature between the RPs. Smaller temperature decreases can be observed in areas where axial spacing between RPs was 10 m or more. This is due not only to the larger axial spacing, but also to the different temperature load that was applied in accordance with the monitored values (Fig. 8). Quantitatively, it is important to note that the temperature did not drop significantly below 0 °C in any of the sediments directly involved in the exploitation or storage of geothermal energy. If this would have occurred, the efficiency of the proposed system would be overloaded, and the long-term sustainability of the resource would be questionable.

The presented results correspond to the transient heat transfer regime at the end of the 10-year simulation period. Due to the temperature load that was applied, which was identical in each year of the simulation, the model only gave information about the temperature fluctuation in the sediments across the simulated years. Therefore, this type of model approach does not provide a long-term view of the decline in sediment temperatures, i.e, an indication of true sustainability. Fig. 13 complements the above results by examining data in the vertical axis at the end of the RP, 300 m from shore. It depicts the simulated sediment temperatures before and after GE exploitation in the final year of the simulation. The black dashed curves show the envelope of thermal fluctuations without GE exploitation, i.e, the origin temperature data

Table 2
Impact area in horizontal axis between RPs.

Distance from shore	Zone	Distance from axis (m)	Temp. drop (°C)
100 m (Axial distance of RPs: 6 m)	RP	0	2.7
	High impact	3	0.8
	Low impact	–	–
	Zero impact	–	–
200 m (Axial distance of RPs: 10 m)	RP	0	2.2
	High impact	1.7	0.6
	Low impact	5	0.2
	Zero impact	–	–
300 m (Axial distance of RPs: 14 m)	RP	0	2
	High impact	1.6	0.5
	Low impact	3.5	0.2
	Zero impact	7	0.1

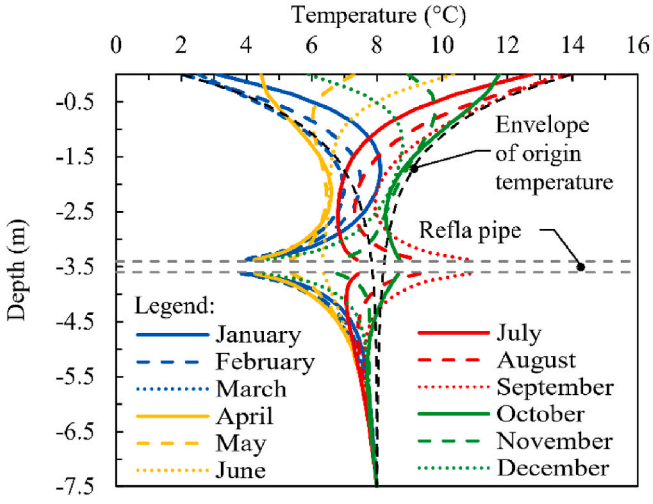

Fig. 13. Temperature distribution in 10th year of simulation in vertical axis of Refla pipe (300 m from shore). (color figure).

depicted in Fig. 7. The colored lines illustrate the seasonal temperature fluctuation during the year with GE exploitation.

4. Conclusions

The aim of this paper was to present the potential and shortcomings of numerical modeling as a tool to verify the operation of an innovative heating system using shallow geothermal energy operating in seabed sediment in Suvilahti, Vaasa, Finland. The numerical analysis was carried out using 2D sections, which, due to the nature of the modeled subject, did not imply significant limitations. It investigated evolution of the sediment temperature during GE exploitation over a period of 10 years, applying a transient heat transfer analysis. The Suvilahti system uses a specific type of Refla coaxial pipe, embedded in the seabed sediments in two 300 m-long, fan-shaped configurations, one approximately 155 m wide, the other 165 m wide. Deposition in the seabed sediments was chosen because seabed temperatures are above 0 °C all year, whereas shallow depths near the shore are seasonally below 0 °C. The average depth of deposition is approximately 3.5 m below the seabed. This relatively modest depth allows the heat gains from the warm seasons to be exploited, but on the other hand, means thermal energy is removed from the system in the cold seasons. This blend of seasonal gains and losses associated with the depth of the system's pipes underpinned the need to carry out a numerical study to define sediment temperature fluctuations without and consequently with exploitation of geothermal energy. Subsequently, the results of temperature monitoring carried out in the Suvilahti system between 2013 and 2016 were used as the applied temperature load for the numerical model. The important thing to be discussed are the limitations of the numerical model. This part summarizes the limits which are mentioned in this study and adds to them a short comment. The fundamental simplifications that are accepted in the model are as follows:

- The temperature load was defined as the "prescribed temperature", which was the most relevant choice, given the monitoring implemented. On the other hand, the prescribed temperature load imposed some limitations in terms of defining a sustainable amount of geothermal energy that can be extracted. Thus, the numerical model, due to its design, provided information mainly on the temperature fluctuation during the geothermal energy exploitation in the subject area. The aim was to check whether there would be significant undercooling below 0 °C in some parts of the system, which would reduce the efficiency of GE utilization. In the short term, this would not represent a fundamental flaw in the design, but rather would highlight the possibility of compromising the sustainability of the GE resource while maintaining the current heating and cooling regime.
- The model is an approximation of real situation only. In this analysis, the real 3D situation is reduced to a planar (2D) model. The 2D model presented in this article is a compromise between an acceptable simplification of real situation and a higher computation time of 3D model. The 2D model simulates the situation in the plane situated in three different axial distances from shore. If it is necessary to obtain results from other distances, it is necessary to use linear interpolation. Boundary condition - a certain simplification is the use of top boundary condition at the seabed for all solved models (2D cross-section). Presumption: this temperature is variable only during the season, not with location, because the seawater flow ensures a constant temperature across the whole seabed.
- Heat transport in sediment is ensured by conduction - groundwater flow is not considered in the calculation, because the sediments are soils with quite low permeability.

The following conclusions can be drawn from the results of the presented numerical study: temperature as a consequence of energy exploitation. The basis for the comparison is the year's average sediment temperature at each location:

- A temperature reduction of more than 10 % of the original sediment temperature occurs within 1.6 m–1.7 m in a radial horizontal direction of each pipe. At a distance of up to 100 m from the shore, where the axial distance of the RPs is less than 6 m, there is a high impact (more than 10 %) in the entire area between the RPs. This information is significant for the design of new similar systems using RPs in similar geological and meteorological conditions.
- A decrease from original sediment temperature of less than 2 % occurred at a radial distance of 3.5 m–5 m around RPs, and was observed at a distance of 100 m–300 m from shore. This conclusion can be used to determine the optimal axial distance between RPs, i.e., 10 m–14 m, if implementing a new system with RPs in a parallel alignment. A considerable area of sediments between RPs was thermally affected by less than 0.1 °C where axial distance was 14 m, indicating that greater axial distance between RPs is unnecessary.
- The results suggest the first third of the RPs' length, i.e., 0 m–100 m from shore, are of questionable effectiveness. This conclusion stems from the results of the temperature distribution at a distance of 100 m from the shore: it can be assumed that the influence of temperature loading in the sediments will be even higher nearer to the shore. When estimating the amount of extractable energy (which this study does not address), it is advisable not to consider this area.
- It is also clear from the results that, if the current working regime is maintained, there is no significant reduction of the temperature below freezing point in the subject areas. Therefore, it can be argued that the installation's extraction of geothermal energy offers long-term sustainability.

CRediT authorship contribution statement

Marek Mohyla: Conceptualization, Methodology, Writing – original draft, preparation, Software, Visualization. **Eva Hrubesova:** Data curation, Writing – original draft, preparation. **Birgitta Martinkauppi:** Supervision, Validation, Reviewing. **Anne Mäkiranta:** Measurements, Writing – original draft, preparation. **Ville Tuomi:** Writing – review & editing.

Declaration of competing interest

The authors declare that they have no known competing financial interests or personal relationships that could have appeared to influence the work reported in this paper.

Acknowledgment

The authors thank the following projects for their financial support: 1) European Commission, HORIZON 2020, project No. 856670 Geothermal Energy in Special Underground Structures and 2) conceptual and specific research development at VSB - Technical University of Ostrava in 2021.

References

[1] B.W. Ang, Bin Su, Carbon emission intensity in electricity production: a global analysis, Energy Pol. 94 (2016) 56–63.
[2] Juan lin, Yijuan Shen, Xin Li, Amir Hasnaoui, BRICS carbon neutrality target: measuring the impact of electricity production from renewable energy sources and globalization, J. Environ. Manag. 298 (2021).
[3] Kim Hanh Nguyen, Makoto Kakinaka, Renewable energy consumption, carbon emissions, and development stages: some evidence from panel cointegration analysis, Renew. Energy 132 (2019) 1049–1057.
[4] Mita Bhattacharya, Sudharshan Reddy Paramati, Ilhan Ozturk, Sankar Bhattacharya, The effect of renewable energy consumption on economic growth: evidence from top 38 countries, Appl. Energy 162 (2016) 733–741.
[5] W. Yueming, et al., Development status of advanced thermal power technology and low-carbon path of China's thermal power industry, in: 2021 IEEE Sustainable Power and Energy Conference (iSPEC), 2021, pp. 2049–2066.
[6] A.C. Marques, J.A. Fuinhas, J.P. Manso, A quantile approach to identify factors promoting renewable energy in European countries, Environ. Resour. Econ. 49 (3) (2011) 351–366.

[7] R. O'Connell, A. Phadke, M. O'Boyle, C.T. Clack, P. Denholm, B. Ernst, Carbon-free energy: how much, how soon?, in: IEEE Power and Energy Magazine, vol. 19, 2021, pp. 67–76, 6.
[8] T.O. Azari, V.S. Tabar, T. Amraee, Multi-objective expansion planning of renewable resources in distribution systems towards achieving a pollution free structure, in: 2022 30th International Conference on Electrical Engineering (ICEE), 2022, pp. 170–174.
[9] J. Kang, Y. Wei, L. Liu, R. Han, B. Yu, J. Wang, Energy systems for climate change mitigation: a systematic review, Appl. Energy 263 (2020).
[10] R.C. Pietzcker, S. Osorio, R. Rodrigues, Tightening EU ETS targets in line with the european green deal: impacts on the decarbonization of the EU power sector, Appl. Energy 293 (2021).
[11] S. Gallego Amores, I. Losa, E-mobility deployment and impact on european electricity networks. Innovation actions needed in the context of the european green deal, in: CIRED Porto Workshop 2022: E-Mobility and Power Distribution Systems, 2022, pp. 651–655.
[12] H. Kulasekara, V. Seynulabdeen, A review of geothermal energy for future power generation, in: 2019 5th International Conference on Advances in Electrical Engineering (ICAEE), 2019, pp. 223–228.
[13] N. Bartels, G. Bussmann, R. Ignacy, Geothermal energy in the context of the energy transition process, in: 2018 International IEEE Conference and Workshop in Óbuda on Electrical and Power Engineering (CANDO-EPE), 2018, pp. 103–108.
[14] John W. Lund, Aniko N. Toth, Direct utilization of geothermal energy 2020 worldwide review, Geothermics 90 (2021).
[15] Stuart J. Self, Bale V. Reddy, Marc A. Rosen, Geothermal heat pump systems: status review and comparison with other heating options, Appl. Energy 101 (2013) 341–348.
[16] Alireza Aslani, Petri Helo, Marja Naaranoja, Role of renewable energy policies in energy dependency in Finland: system dynamics approach, Appl. Energy 113 (2014) 758–765.
[17] A. Mäkiranta, B. Martinkauppi, E. Hiltunen, Seabed Sediment: a Natural Seasonal Heat Storage Feasibility Study, vol. 15, Agronomy research, 2017, pp. 1101–1106, special no. 1.
[18] E. Hiltunen, B. Martinkauppi, L. Zhu, A. Mäkiranta, M. Lieskoski, J. Rinta-Luoma, Renewable, carbon-free heat production from urban and rural water areas, J. Clean. Prod. 153 (2017) 397–404.
[19] N. Girgibo, A. Mäkiranta, X. Lü, E. Hiltunen, Statistical investigation of climate change effects on the utilization of the sediment heat energy, Energies 15 (2) (2022).
[20] A. Mäkiranta, B. Martinkauppi, E. Hiltunen, M. Lieskoski, Seabed sediment as an annually renewable heat source, Appl. Sci. 8 (2) (2018).
[21] G.E. Likens, N.M. Johnson, Measurement and analysis of the annual heat budget for the sediments in two Wisconsin lakes, Limnol. Oceanogr. 14 (1) (1969) 115–135.
[22] S. Golosov, G. Kirillin, A parameterized model of heat storage by lake sediments, Environ. Model. Software 25 (6) (2010) 793–801.
[23] E.A. Birge, C. Juday, H.W. March, The temperature of the bottom deposits of Lake Mendota, A chapter in the heat exchanges of the lake, Trans. Wis. Acad. Sci. 187 (1927). –231.
[24] N.P. Smith, Observations and simulations of water-sediment heat exchange in a shallow coastal lagoon, Estuaries 25 (2002) 483–487.
[25] M.A. Briggs, L.K. Lautz, J.M. McKenzie, A comparison of fibre-optic distributed temperature sensing to traditional methods of evaluating groundwater inflow to streams, Hydrol. Process. 26 (9) (2012) 1277–1290.
[26] Y. Rui, R. Hird, M. Yin, K. Soga, Detecting changes in sediment overburden using distributed temperature sensing: an experimental and numerical study, Mar. Geophys. Res. 40 (3) (2019) 261–277.
[27] A. Mäkiranta, "Distributed Temperature Sensing Method-Usability in Asphalt and Sediment Heat Energy Measurements" Master Thesis, University of Vaasa, 2013. Finland, Available: http://osuva.uwasa.fi/handle/10024/3385.
[28] R. Gu, H.G. Stefan, Year-round temperature simulation of cold climate lakes, Cold Reg. Sci. Technol. 18 (2) (1990) 147–160.
[29] M. Hondzo, C. Ellis, H. Stefan, Vertical diffusion in small stratified lake: data and error analysis, J. Hydraul. Eng. 117 (10) (1991) 1352–1369.
[30] H.E. Welch, M.A. Bergmann, Water circulation in small arctic lakes in winter, Can. J. Fish. Aquat. Sci. 42 (1985) 506–520.
[31] T. Tsay, G.J. Ruggaber, S.W. Effler, C.T. Driscoll, Thermal stratification modeling of lakes with sediment heat flux, J. Hydraul. Eng. 118 (3) (1992) 407–419.
[32] L. Bengtsson, Mixing in ice-covered lakes, Hydrobiologia 322 (1996) 91–97.
[33] X. Fang, H.G. Stefan, Dynamics of heat exchange between sediment and water in a lake, Water Resour. Res. 32 (1996) 1719–1727.
[34] C.G. Scotch, D. Murgulet, J. Constantz, Time-series Temperature Analyses Indicate Conduction and Diffusion Are Dominant Heat-Transfer Processes in Fine Sediment, Low-Flow Streams, vol. 768, Science of The Total Environment, 2021.
[35] J. Acuña, "Distributed Thermal Response Tests – New Insights on U-Pipe and Coaxial Heat Exchangers in Groundwater-Filled Boreholes," Ph.D. Dissertation, KTH School of Industrial Engineering and Management. Division of Applied Thermodynamics and Refrigeration, Stockholm, 2013.
[36] A. Sanguinetti, S. Outcault, E. Alston-Stepnitz, M. Moezzi, A. Ingle, Residential solar water heating: California adopters and their experiences, Renew. Energy 170 (2021) 1081–1095.
[37] Syed Shah Alam, Nik Hazrul Nik Hashim, Mamunur Rashid, Nor Asiah Omar, Nilufar Ahsan, Md Daud Ismail, Small-scale households renewable energy usage intention: theoretical development and empirical settings, Renew. Energy 68 (2014) 255–263.
[38] E. Bjørnstad, Diffusion of renewable heating technologies in households. Experiences from the Norwegian Household Subsidy Programme, Energy Pol. 48 (2012) 148–158.
[39] C. Franceschinis, M. Thiene, R. Scarpa, J. Rose, M. Moretto, R. Cavalli, Adoption of renewable heating systems: an empirical test of the Diffusion of innovation theory, Energy 125 (2017) 313–326.
[40] S. Bahrami, B. Atkin, A. Landin, Enabling the diffusion of sustainable product innovations in BIM library platforms, Journal of Innovation Management 7 (4) (2019) 106–130.
[41] J. Räihä, E. Ruokamo, Determinants of supplementary heating system choices and adoption consideration in Finland, Energy Build. 251 (2021).
[42] M.E. Rogers, Diffusion of Innovations, 5-th ed., Free Press, 2003. ISBN13: 9780743222099.
[43] A. Mäkiranta, J.B. Martinkauppi, E. Hiltunen, Correlation between temperatures of air, heat carrier liquid and seabed sediment in renewable low energy network, Agron. Res. 14 (2016) 1191–1199, special no. 1.
[44] S. Valpola, Sedimentin Lämpötilamittaukset Vaasan Suvilahden Edustalla, Geological Survey of Finland, 2006. Available only in Finnish. Public research report.